Autonomous Vehicle Control for Emergency Maneuvers: The Effect of Topography*

John Subosits[1,2] and J. Christian Gerdes[1]

Abstract— **When attempting to drive collision-free paths in emergency situations, automobiles are limited by the amount of force their tires can produce through friction. A road's topography affects the tire forces, so the ability of an autonomous vehicle to follow a desired path depends on the shape of the path in three, not two, dimensions. In this paper, a model that captures the effects of road topography on tire forces is derived and used to compute the speeds at which a given path can be followed. Experimental evidence is used to support the conclusion that accounting for topography, particularly the vertical curvature of the road, is critical for good path tracking performance even with a conservative estimate of maximum friction.**

I. INTRODUCTION

A conventional approach to the motion planning problem in the robotics community is to use a path planner with a path following controller operating beneath it. For automobiles, the limited friction of the tires restricts the set of feasible paths available to a moving vehicle. These limits become extremely important when attempting to avoid collisions or other unexpected hazards by using all the control force available. The maximum force capability of the tires and the force required to follow a path at a given speed can be significantly influenced by the road surface's three dimensional shape or topography. For an autonomous vehicle to have the best chance of avoiding a collision, it must have a good model for the forces required and the force potential offered by an intended path.

One way to account for friction limitations is to separate trajectory generation from path planning. Once the path has been fixed, choosing a speed profile, the velocity as a function of distance along that path, determines the trajectory. Minimum time speed profiles for aircraft and automobiles have been found using both semi-analytical methods [1][2] and convex optimization [3]. Experiments conducted at the limits of friction with an autonomous vehicle have demonstrated the effectiveness of the semi-analytical method [4]. While the inclusion of topography in trajectory generation has been limited, some path planning work has included the effect of topography on a vehicle's limits. Simulation results have been used to make recommendations for safer roadway design specifications [5], but the question of how to best drive existing roads with significant topography remains unanswered. The effects of topography have been analyzed by the vehicle dynamics community [6], but have yet to be used for autonomous vehicle control. This work analyzes the influence of road topography on the minimum time trajectory.

This paper presents a model which captures the interacting effects of road features such as bank, grade, and hill crests. The resulting three-dimensional bicycle model is as amenable to use in rapid computations as the simpler models used previously which include few or no topographical effects. The path tracking performance of an autonomous vehicle operating near the limits of friction demonstrates the benefit of using a richer model. Using the model for the effects of topography presented here significantly reduces deviation from the desired path.

This paper begins with a purely conceptual description of the effects of topography on a vehicle operating near its limits. The resulting intuition is then formalized into a three-dimensional bicycle model. The initial six degree of freedom rigid body model is simplified to yield a model with one degree of freedom in which the friction limits of each axle can be considered separately. A brief example of the model's use in the calculation of the minimum time trajectory follows. This trajectory is then used as a reference for an autonomous vehicle. The experimental results obtained are presented to support the conclusion that accounting for all effects of road topography allows the vehicle to be pushed closer to its true limits.

II. VEHICLE DYNAMICS

A. Load Transfer Concept

A crucial concept in vehicle dynamics is that of load transfer. When a vehicle is stationary on a flat surface, the load on each tire is determined by the vehicle's mass and center of gravity location. However, when the vehicle is accelerating, the normal load on each tire changes, changing the maximum force each tire can generate through friction. For example, when a vehicle brakes while traveling in a straight line, forces acting at ground level through the contact patches of the tires slow the vehicle. These forces also exert a torque about the vehicle's center of gravity which must be balanced by an increase in the normal load on the front wheels and a corresponding decrease at the rear.

This longitudinal load transfer affects the the acceleration capabilities of the vehicle as a whole. While braking, the rear tires are unloaded, reducing the amount of lateral force they can generate as shown by the asymmetry of the rear tire curve in Fig. 1. This loss of load makes it easier to demand too much lateral force from the rear tires while

*This research is supported by the Electronics Research Laboratory of Volkswagen of America (ERL).

[1]Department of Mechanical Engineering at Stanford University, Stanford, California, USA.

[2]This is the corresponding author. subosits@stanford.edu

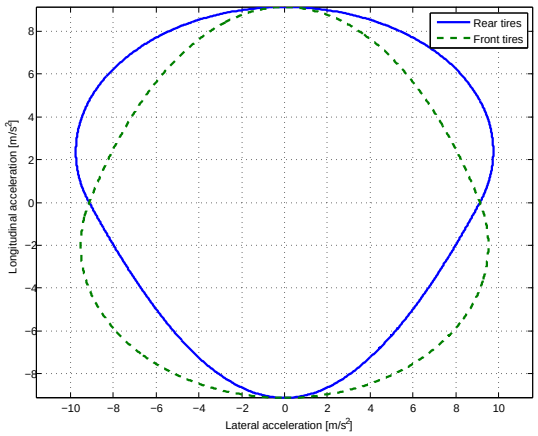

Fig. 1. Accleration limits of the vehicle on a level surface.

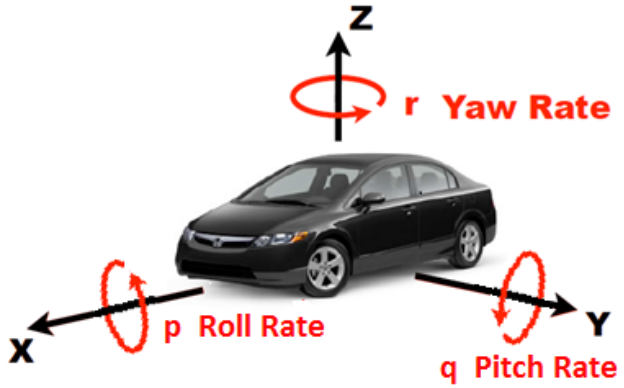

Fig. 2. Orientation of vehicle fixed axes and definition of angular velocity components.

cornering, possibly leading to a loss of control and a spin. Similarly, when accelerating and turning, the front tires are more likely to slide. While each tire can generate roughly the same amount of force in any direction, the maximum possible acceleration for the vehicle under a combination of longitudinal and lateral acceleration is less than during pure longitudinal or lateral acceleration because the vehicle is constrained by the more restrictive of the front and rear tire limits. The size of this effect can only be assessed by accurately modeling the normal load on the tires.

A non-level road surface also affects the acceleration limits of the vehicle. A downhill grade increases maximum acceleration at the expense of maximum deceleration while reducing maximum steady-state lateral acceleration since braking is required to maintain speed. While grade shifts the limits in Fig. 1 vertically, banking shifts them horizontally. While these effects are well understood, the effect of vertical curvature, the change in grade seen by the vehicle, has been less studied. Vertical curvature can have a large effect on tire normal loads, decreasing the magnitude of the vehicle's acceleration limits when cresting hills and increasing it when traveling through sags between them. Accounting for vertical curvature can be as important as modeling the effects of bank and grade when designing an autonomous vehicle controller.

B. Dynamic Model

We present a three-dimensional bicycle model which captures the effects of bank, grade, and vertical curvature discussed above. Modeling the vehicle as a single rigid body and working in an inertial earth-fixed frame, the position and velocity of the vehicle's center of gravity are given by

$$\vec{r} = x(s)\hat{i} + y(s)\hat{j} + z(s)\hat{k} \tag{1}$$

$$\vec{v}_I = \frac{dx}{ds}\frac{ds}{dt}\hat{i} + \frac{dy}{ds}\frac{ds}{dt}\hat{j} + \frac{dz}{ds}\frac{ds}{dt}\hat{k} \tag{2}$$

where s is the distance along the three dimensional path. Applying the product rule, the acceleration at a given point is given by

$$\vec{a}_I = V^2\left(\frac{d^2x}{ds^2}\hat{i} + \frac{d^2y}{ds^2}\hat{j} + \frac{d^2z}{ds^2}\hat{k}\right) + \dot{V}\left(\frac{dx}{ds}\hat{i} + \frac{dy}{ds}\hat{j} + \frac{dz}{ds}\hat{k}\right) \tag{3}$$

where V^2 and $\dot{V}$ are the square of the vehicle's speed and scalar acceleration along the path. V^2 and $\dot{V}$ multiply vectors normal and tangential to the path.

Next the angular motions of the vehicle are considered in the non-inertial body-fixed frame shown in Fig. 2. If it is assumed that suspension motions and vehicle sideslip can be neglected, the longitudinal axis of the vehicle is always tangent to the path. Therefore, the roll, pitch, and yaw angles of the vehicle are the same as the bank, grade, and heading of the path, and the vehicle's orientation can be deduced from only the vehicle's position along the path and the the path's geometry. This simplification makes the problem tractable.

The orientation in space of the vehicle and of the vector tangent to the path are given by a set of Euler angles,

$$\Theta = \begin{pmatrix} \phi \\ \theta \\ \psi \end{pmatrix} \tag{4}$$

which denote respectively the bank, grade, and heading. Rotations follow the order of yaw, pitch, and roll according to the Tate-Bryant convention. Hence, the angular velocity of the vehicle in the body frame is given by

$$\omega_B = \begin{pmatrix} p \\ q \\ r \end{pmatrix} = L_I^B \dot{\Theta} \tag{5}$$

where

$$L_I^B = \begin{pmatrix} 1 & 0 & -\sin\theta \\ 0 & \cos\phi & \sin\phi\cos\theta \\ 0 & -\sin\phi & \cos\phi\cos\theta \end{pmatrix} \tag{6}$$

is the angular rate transformation matrix that relates the Euler angle rates to the angular velocity in the body frame.

The equation describing rotational motion is

$$\sum M_B = I_B\dot{\omega}_B + \omega_B \times (I_B\omega_B) \tag{7}$$

$$= I_B(\dot{L}_I^B\dot{\Theta} + L_I^B\ddot{\Theta}) + \omega_B \times I_B\omega_B \tag{8}$$

where I_B is the inertia tensor of the vehicle expressed in the body frame. As with the forces acting on the vehicle, by using the chain rule, the necessary moments at a point along the path can be expressed as a linear function of the the speed squared and the acceleration:

$$\sum M_B = M_{\dot{V}}\dot{V} + M_{V^2}V^2 \tag{9}$$

where

$$M_{\dot{V}} := I_B L_I^B \frac{d\Theta}{ds} \tag{10}$$

and

$$M_{V^2} := I_B \frac{dL_I^B}{ds}\frac{d\Theta}{ds} + I_B L_B^I \frac{d^2\Theta}{ds^2} + (L_I^B \frac{d\Theta}{ds}) \times (I_B L_I^B \frac{d\Theta}{ds}). \tag{11}$$

M_{V^2} and $M_{\dot{V}}$ depend only on the path geometry and the inertia tensor.

For the results above to be useful for the speed control of vehicles, it is necessary to determine the tire forces that arise from a given trajectory. It is simplest to express the forces acting on the vehicle in the body frame. To express the acceleration coefficients in (3) similarly, an Euler angle rotation matrix, $M_I^B(\phi(s), \theta(s), \psi(s))$ is defined so that

$$\sum F_B = m M_I^B \vec{a}_I. \tag{12}$$

$$= m(A_{V^2}V^2 + A_{\dot{V}}\dot{V}) \tag{13}$$

where

$$A_{V^2} := M_I^B(\frac{d^2x}{ds^2}, \frac{d^2y}{ds^2}, \frac{d^2z}{ds^2})^\top \tag{14}$$

and

$$A_{\dot{V}} := M_I^B(\frac{dx}{ds}, \frac{dy}{ds}, \frac{dz}{ds})^\top = (1,0,0)^\top. \tag{15}$$

The last equality holds because of the assumption that the vehicle is aligned with the path at all times.

The vehicle is modeled using a bicycle model in which the forces generated by the tires on a given axle are lumped together as shown in Fig. 3. This simplification works because the friction limits chosen for each axle implicitly include steady-state lateral weight transfer effects. Replacing $\sum F_B$ in (13) and $\sum M_B$ in (9) by the forces and moments acting on the vehicle and solving for the tire forces gives the following expressions. Note that γ denotes the ratio of drive or braking torque between the front and rear axles, and $L = a + b$ is the vehicle's wheelbase. For the vehicle to remain on the path,

$$F_{xf} = \gamma \frac{m(\dot{V} - g_x) + \frac{1}{2}\rho C_D A V^2}{1+\gamma} \tag{16}$$

$$F_{xr} = \frac{m(\dot{V} - g_x) + \frac{1}{2}\rho C_D A V^2}{1+\gamma} \tag{17}$$

$$F_{yf} = \frac{bm}{L}(A_{V^2,y}V^2 - g_y) + \frac{1}{L}(M_{V^2,z}V^2 + M_{\dot{V},z}\dot{V}) \tag{18}$$

$$F_{yr} = \frac{am}{L}(A_{V^2,y}V^2 - g_y) - \frac{1}{L}(M_{V^2,z}V^2 + M_{\dot{V},z}\dot{V}) \tag{19}$$

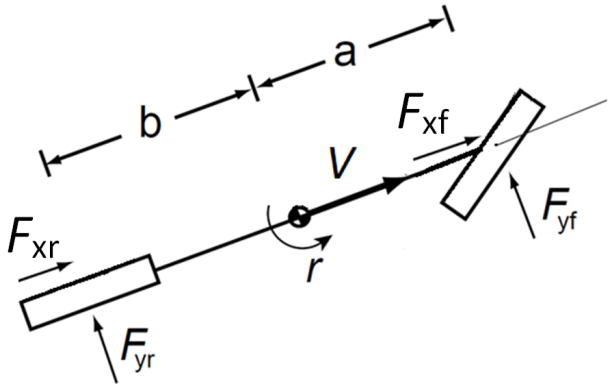

Fig. 3. Bicycle model schematic showing symbol definitions.

$$F_{zf} = \frac{1}{L}[mb(A_{V^2,z}V^2 - g_z) - h(F_{xf} + F_{xr}) - (M_{V^2,y}V^2 + M_{\dot{V},y}\dot{V})] \tag{20}$$

$$F_{zr} = \frac{1}{L}[ma(A_{V^2,z}V^2 - g_z) + h(F_{xf} + F_{xr}) + (M_{V^2,y}V^2 + M_{\dot{V},y}\dot{V})] \tag{21}$$

where the subscripts indicate the component of each vector. For example, $M_{V^2,y}$ is the second component of M_{V^2} and represents the required moment about the y-axis for a given speed. g_i is the component of the gravitational acceleration acting along the i-axis in the body frame. The aerodynamic drag on the car is given by $\frac{1}{2}\rho C_D A V^2$.

Examining the expressions for normal force, F_z, reveals the effects of vertical curvature. At the crest of a hill, $A_{V^2,z}$ is negative and causes a decrease in the normal load on each axle proportional to V^2. Conversely, $M_{V^2,y}$ and $M_{\dot{V},y}$ are both positive and model the torque that aligns the car to the changing slope of the road. The last term differs only in sign between the two expressions and changes the front/rear load distribution, increasing the likelihood that the front tires will saturate when cresting hills.

III. SPEED PROFILE GENERATION

Determining a speed profile for the vehicle requires translating the capabilities of the tires to generate forces into acceleration limits for the vehicle and then into maximum safe speeds. Using a friction circle model for the tires, the constraints are given by

$$F_{xi}^2 + F_{yi}^2 \leq (\mu F_{zi})^2; \;\; i = f, r. \tag{22}$$

where μ is the effective coefficient of friction between the tire and the road. Since each term in the above equation is an affine function of $\dot{V}$ and V^2, fixing either $\dot{V}$ or V^2 results in a quadratic equation in the other variable. The value of the independent variable that saturates each tire can then be determined analytically.

A minimum time trajectory can be found by the following method which is similar, but not identical, to other proposed algorithms which have been proven to give an optimal result

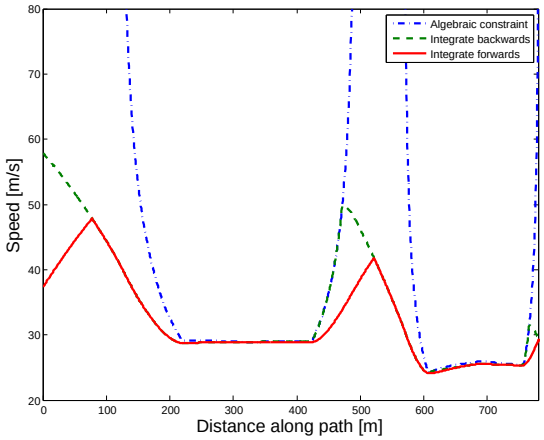

Fig. 4. A portion of the intermediate and final results of the speed profile computation algorithm for Turns 2 and 3 of Thunderhill. Full topography information was used in the computation.

[1][2]. The algorithm consists of the following steps. Find the maximum velocity at each of a number of points along the path. The longitudinal acceleration can either be fixed at zero for this computation or varied iteratively at each point in order to achieve the highest possible velocity. Compute the velocities that saturate the front and rear tires using (22). The smaller value is the maximum safe speed at that point.

Once the point-wise constraints (Algebraic constraint in Fig. 4) have been determined, enforce the differential constraints. To minimize time, deceleration for approaching corners must be of the largest possible magnitude. Making the approximation that deceleration is constant over each small spatial step of length d, the speed at the previous point is given by

$$V_{n-1}^2 = V_n^2 - 2a_{decel,max}d. \tag{23}$$

The possible deceleration must be computed for each tire and the more restrictive value used. For a closed path, the integration begins from the point of minimum safe speed. When the effect of road topography is included, this point of minimum speed is not necessarily where the horizontal radius is smallest. For open paths that have distinct start and finish points, integrate backwards from the finish. If at any point the velocity arrived at by integration is greater than the maximum allowable, use the smaller value as the initial condition for the next integration step.

After completing the backwards integration over the entire path, perform another integration in the forwards direction beginning from the start of an open path or from the slowest point on a closed path. Optionally, engine power constraints can be incorporated into this step to give a trajectory that the vehicle can achieve. The final result for a portion of the Thunderhill circuit is shown in Fig. 4 (Integrate forwards). The parameters used in the computation are given in Table I.

TABLE I
VEHICLE PARAMETERS

Parameter	Value	Units
m	1648	kg
I_{xx}	500	$\mathrm{kg \cdot m^2}$
I_{yy}	1800	$\mathrm{kg \cdot m^2}$
I_{zz}	2250	$\mathrm{kg \cdot m^2}$
I_{xz}	0	$\mathrm{kg \cdot m^2}$
a	1.04	m
b	1.42	m
h	0.61	m
$\frac{1}{2}\rho C_D A$	0.36	$\mathrm{kg \cdot m^{-1}}$
μ	0.85	unitless

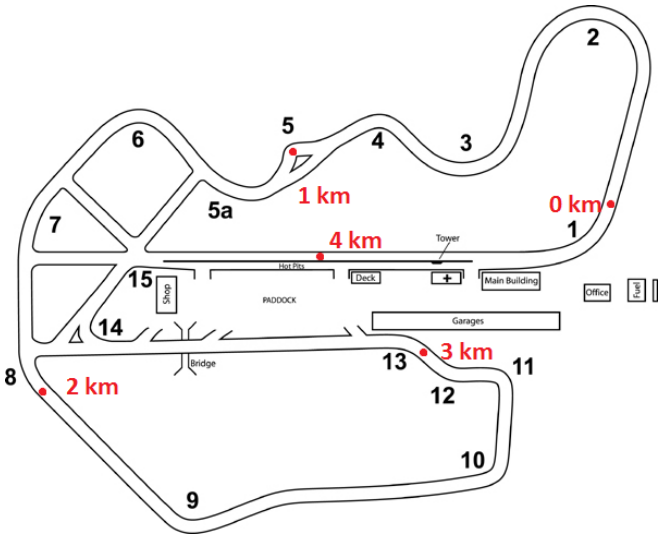

Fig. 5. Map of Thunderhill Raceway showing turn numbers and distance along the reference path.

IV. EXPERIMENTAL RESULTS

Experimental results obtained by testing a fully autonomous Audi TT-S at Thunderhill Raceway, a moderately hilly circuit, in Willows, CA indicate that accounting for the various topographic effects presented is important for good path tracking performance near the limits of friction. Minimum time travel of a racing line serves as an appropriate proxy for emergency maneuvers since good performance of either requires using all or nearly all the available friction force. In addition to the importance of bank and grade on a vehicle's ability to track a path documented elsewhere [5], the importance of accounting for vertical curvature is demonstrated here. The fifth turn of the Thunderhill circuit, a sharp left hand turn at the crest of a hill, provides a perfect example.

A. Path Geometry

Two approaches were used to obtain the terms used to compute the coefficients appearing in the tire force equations, (16) through (21). The heading angle and its derivatives are drawn directly from the two-dimensional representation of the desired path. The curvature of the path is known at every point since the path is represented as a sequence of clothoid segments whose curvatures vary linearly with distance [7].

Fig. 6. Autonomous TT-S, nicknamed Shelley, negotiating Turn 5. Photo credit: Vincent Laurense.

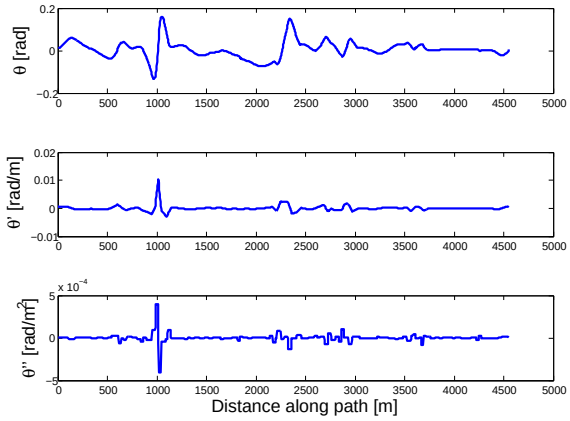

Fig. 7. Grade angle and its derivatives on the Thunderhill circuit.

Measurements of the road's bank and grade were taken by driving slowly along the desired path in a car equipped with a high precision GPS and an inertial measurement unit. The collected data were then differentiated using a total variation diminishing method similar to that proposed by Chartrand [8]. The resulting measurements of bank and grade and their derivatives are shown in Figs. 7 and 8.

The topography of the circuit is mostly consistent with design guidelines for public roads. To facilitate drainage, most of the circuit is banked to the left by an amount similar to that used on interstate highways [9]. This fact generally increases cornering speeds slightly. The maximum grade of the road exceeds that permitted on interstate highways, but is comparable to that seen on local roads in hilly areas [9]. The vertical curvature, θ', seen at Turn 5 exceeds that permitted in recognized standards limiting the sharpness of vertical curves at hill crests in order to allow drivers adequate sight distance [9]. Nevertheless, to be safe, autonomous vehicles must drive capably on roads that do not meet specifications or even off the road entirely if the situation requires.

The derivatives of the spatial coordinates appearing in (3) are computed from the measured Euler angles according to the following relations and their spatial derivatives.

$$\frac{dx}{ds} = \cos\theta\cos\psi; \quad \frac{dy}{ds} = \cos\theta\sin\psi; \quad \frac{dz}{ds} = -\sin\theta$$

The topography data are then combined with the known parameters of the test vehicle for speed profile determination.

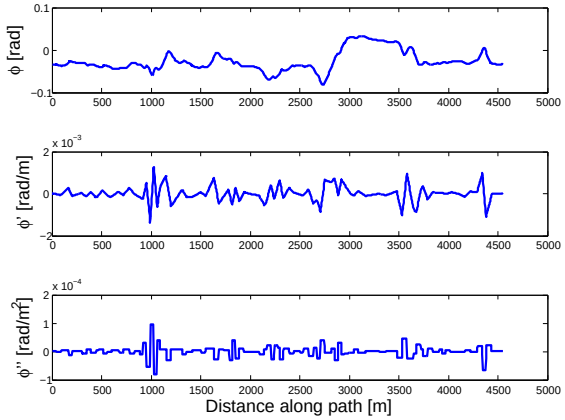

Fig. 8. Bank angle and its derivatives on the Thunderhill circuit.

B. Steering Controller

The vehicle uses a steering controller which achieves vehicle stability and close tracking of the reference path both near the limits of friction and at more sedate speeds [10]. Expected steady-state vehicle sideslip is incorporated into the feedforward control law to keep the vehicle's velocity tangent to the path. The feedback controller uses a lookahead scheme to regulate the lateral error from the path at a fixed distance ahead of the car.

C. Experimental data

Desired speed profiles were computed for a path around the Thunderhill circuit for two cases. In the first case, "With curvature compensation," all topographic data were incorporated into the computation of the speed profile. In the second, the derivatives of the road grade, θ' and θ'', were artificially set to zero, but the effect of road grade itself was still included. The vehicle aimed to maintain accelerations of 0.85 g's which is approximately 92% of its true limit. During the test, the computed speed profile served as a reference for the vehicle's speed controller.

A comparison of the vehicle's path through Turn 5 when following each of the speed profiles is shown in Fig. 9. The portion of the path shown in the map corresponds to the other data presented. The interval begins when the path begins to turn left and ends 20 m after it straightens out. Examining the north and east positions of the vehicle shows immediately that the vehicle is having difficulty tracking the path when the vertical curvature of the road is ignored even though the maximum difference between the intended speed profiles is less than 2 m/s. Fig. 10 shows the two desired speed profiles and the measured velocities during the tests.

Fig. 11 makes the effects more clear. The path tracking error is reduced from a maximum of 1.30 m to a maximum of 0.37 m when vertical curvature is included in the computation. Furthermore, the path deviation is to the inside of the turn indicating that this error arises from imperfect performance of the steering control not a lack of available

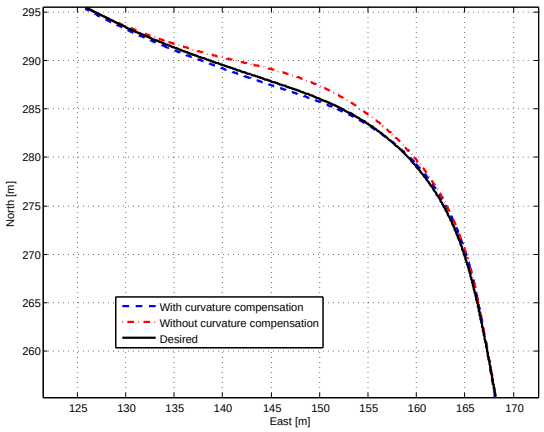

Fig. 9. Spatial location of the two experimental trajectories compared to the desired path.

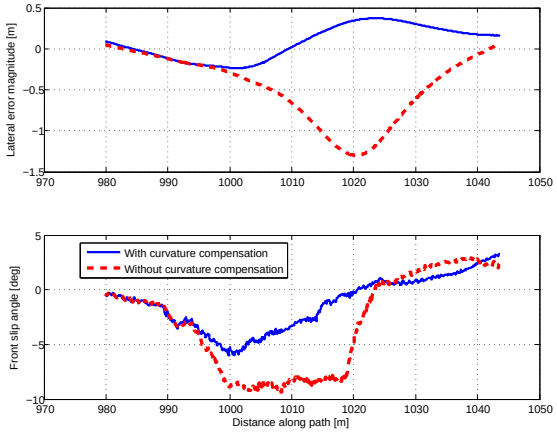

Fig. 11. The combination of the car traveling to the outside of the path and the large sustained front slip angle indicate significant understeer.

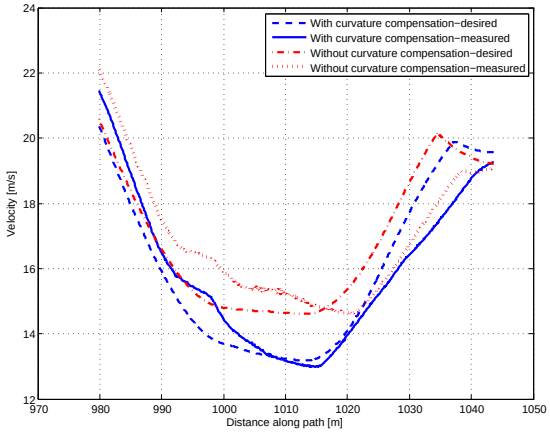

Fig. 10. Desired and measured speed profiles for the two trials.

force. In contrast, the deviation to outside of the path when vertical curvature is ignored is the result of limit understeer caused by exceeding the friction capabilities of the front tires. The measured front slip angles support this assessment; In the case without curvature compensation the front slip angle is large and sustained while the lateral error grows. This fact indicates that the tires have exceeded the available friction, so the car fails to turn and runs wide even though the steering wheel is turned sufficiently.

V. CONCLUSIONS

Considering a full model for the dynamics of a rigid vehicle that is following a predetermined path can significantly improve path tracking performance when operating near the friction limits. These effects are not confined to the racetrack, but are significant for emergency maneuvers on public roads. Using a unified framework ensures that all effects and their interactions are properly captured. Future work will use the minimum time trajectories generated by the method described here to aid the optimization of racing lines on hilly tracks. Accounting for topography at the path design stage allows the car to take advantage of the road topography rather than simply react to it which should result in faster laptimes and safer routes.

ACKNOWLEDGMENT

The authors would like to thank Dynamic Design Lab colleagues Paul Theodosis, Joseph Funke, and John Kegelman for their feedback and interest over the course of the project. The staff of Thunderhill Raceway Park made testing possible. John Subosits is supported by a Stanford Graduate Fellowship through the Technology Licensing Office.

REFERENCES

[1] Y. Zhao and and P. Tsiotras, "Time-optimal path following for fixed-wing aircraft," *AIAA J. of Guidance, Control, and Dynamics*, vol. 36, no. 1, pp. 83-95, Jan.-Feb., 2013.

[2] E. Velenis and P. Tsiotras,"Minimum-time travel for a vehicle with acceleration limits: theoretical analysis and receding-horizon implementation," *J. of Optimization Theory and Applicat.*, vol. 138, no. 2, pp. 275-296, Aug., 2008.

[3] T. Lipp and S. Boyd, "Minimum-time speed optimisation over a fixed path," *Int. J. of Control*, to be published.

[4] K. Kritayakirana and J. C. Gerdes, Autonomous vehicle control at the limits of handling, Int. J. of Vehicle Autonomous Syst., vol. 10, no. 4, pp. 271-296, 2012.

[5] T. Varunjikar, "Design of horizontal curves with downgrades using low-order vehicle dynamics models," M.S. thesis, Dept. Mech. Eng., Penn. State Univ., State College, PA, 2013.

[6] R. N. Jazar, *Vehicle Dynamics*. New York, NY: Springer, 2014, ch. 2.

[7] P. A. Theodosis and J. C. Gerdes, "Generating a racing line for an autonomous racecar using professional driving techniques," in *Proc. ASME Dynamic Systems and Control Conf.*, Arlington, VA, 2011, pp. 2:853-860.

[8] R. Chartrand, "Numerical differentiation of noisy, nonsmooth data," *ISRN Applied Math.*, vol. 2011, 2011.

[9] *A Policy on Geometric Design of Highways and Streets*, 4th ed., American Assoc. of State Highway and Transportation Officials, Washington, D.C., 2001.

[10] N. R. Kapania and J. C. Gerdes, "An Autonomous Lanekeeping System for Vehicle Path Tracking and Stability at the Limits of Handling," presented at the 12th Int. Symp. on Advanced Vehicle Control, Tokyo, 2014.